


Cs $62D_J$ Rydberg-atom macrodimers formed by long-range multipole interactionXiaoxuan Han,^{1,2} Suying Bai,^{1,2} Yuechun Jiao,^{1,2} Liping Hao,^{1,2} Yongmei Xue,^{1,2} Jianming Zhao,^{1,2,*} Suotang Jia,^{1,2} and Georg Raithel^{1,3,*}¹State Key Laboratory of Quantum Optics and Quantum Optics Devices, Institute of Laser Spectroscopy, Shanxi University, Taiyuan 030006, China²Collaborative Innovation Center of Extreme Optics, Shanxi University, Taiyuan 030006, China³Department of Physics, University of Michigan, Ann Arbor, Michigan 48109-1120, USA (Received 17 September 2017; published 9 March 2018)

Long-range macrodimers formed by D -state cesium Rydberg atoms are studied in experiments and calculations. Cesium $[62D_J]_2$ Rydberg-atom macrodimers, bonded via long-range multipole interaction, are prepared by two-color photoassociation in a cesium atom trap. The first color (pulse A) resonantly excites seed Rydberg atoms, while the second (pulse B, detuned by the molecular binding energy) resonantly excites the Rydberg-atom macrodimers below the $[62D_J]_2$ asymptotes. The molecules are measured by extraction of autoionization products and Rydberg-atom electric-field ionization, and ion detection. Molecular spectra are compared with calculations of adiabatic molecular potentials. From the dependence of the molecular signal on the detection delay time, the lifetime of the molecules is estimated to be 3–6 μ s.

DOI: [10.1103/PhysRevA.97.031403](https://doi.org/10.1103/PhysRevA.97.031403)

Recently, molecules involving one or more Rydberg excitations have attracted considerable attention due to their unusual properties. These include exotic adiabatic potentials, vibrational levels that reveal details of the potentials, and unexpected, large permanent electric dipole moments in homonuclear molecules. Two kinds of Rydberg molecules with distinct binding mechanisms have been observed: Rydberg-ground and Rydberg-Rydberg macrodimers. Rydberg-ground molecules, consisting of a Rydberg atom bound to a ground-state atom via a low-energy electron scattering mechanism, include the so-called trilobite molecules [1], which are due to 3S -wave-dominated scattering, and the butterfly molecules [2,3], which are due to a 3P -wave resonance. Rydberg-ground molecules have been experimentally observed for Rydberg S [4,5], P [6], and D states [7,8], and for high-angular-momentum states [9–13]. Molecules consisting of two Rydberg atoms, bound by long-range electrostatic interactions, have been predicted [14] and observed [15–17]. Rydberg-Rydberg macrodimers have bond lengths $\gtrsim 4n^2$, generally exceeding the LeRoy radius, and therefore have negligible exchange interaction. Deiglmayr *et al.* have prepared Cs macrodimer molecules near the nS - $n'F$ and $[nP]_2$ asymptotes for $22 \leq n \leq 32$ [16], and $43P$ - $44S$ [17] molecules bound by long-range dipolar interaction.

Here we observe Cs $[62D_J]_2$ macrodimers on the red-detuned side of the $62D_J$ atomic resonances. We excite the molecules via two-step, two-color photoassociation using two sets of laser pulses, as sketched in Fig. 1(a). Seed Rydberg atoms, denoted as A atoms, are resonantly excited from the ground state using a laser-pulse pair labeled A . The A pulses are two-photon resonant with the interaction-free Rydberg level $|r\rangle = 62D_J$. The 510-nm component of the second laser pulse pair, labeled B , is detuned relative to that of pulse pair

A by an amount equal to the molecular binding energy. The 852-nm components of pulse pairs A and B have the same frequency. The B pulses excite Rydberg atoms close to the seed atoms (A atoms), at a distance where metastable $[62D_J]_2$ macrodimers exist. Owing to the doubly resonant character of this two-color photoassociation scheme, the excitation rate is greatly enhanced in comparison with that of single-color photoassociation.

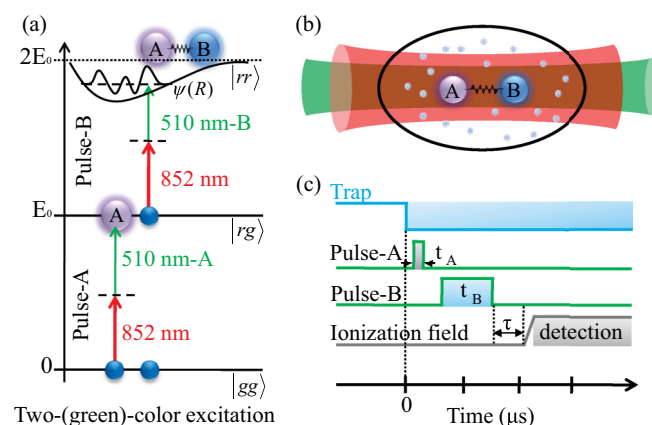


FIG. 1. Level diagram and sketch of a vibrational wave function (a) and schematic of the experiment (b) for two-color double-resonant excitation of $[62D_J]_2$ Rydberg-atom macrodimers. The 852- and 510-nm excitation beams counterpropagate through a cold Cs atom cloud. The pulse pair A resonantly excites seed Rydberg atoms (atom A). To study Rydberg-atom macrodimers, the frequency of the 510-nm component of the pulse pair B is scanned relative to the atomic resonance. (c) Timing sequence. After switching off the MOT beams, we sequentially apply the A and B pulses. An optional wait time $\tau \lesssim 40 \mu$ s between the B pulses and detection allows us to study molecular decay.

*Corresponding authors: zhaojm@sxu.edu.cn; graithel@sxu.edu.cn

The experiment is performed in a Cs magneto-optical trap (MOT) with a temperature $\sim 100 \mu\text{K}$, and peak density $\sim 10^{10} \text{ cm}^{-3}$. After switching off the MOT beams, we apply the photoassociation pulses *A* and *B*, as sketched in Figs. 1(a) and 1(b). The MOT magnetic field is always on. The timing diagram is shown in Fig. 1(c). The lower-transition laser (852 nm, Toptica DLpro, $\sim 100 \text{ kHz}$ linewidth) is stabilized to the $|6S_{1/2}, F=4\rangle (|g\rangle) \rightarrow |6P_{3/2}, F'=5\rangle (|e\rangle)$ transition using polarization spectroscopy [18], and is shifted off-resonance from $|e\rangle$ by 220 MHz using a double-pass acousto-optic modulator (AOM). The upper-transition laser (510 nm, Toptica TA SHG110, $\sim 1 \text{ MHz}$ linewidth) is stabilized to a $62D_J$ Rydberg transition using a Rydberg EIT reference signal [19], and double passed through another AOM. For the pulse pair *A*, the 510-nm AOM frequency is set to resonantly excite the seed Rydberg atoms (*A* atoms). During the subsequent *B* pulse, the 510-nm AOM frequency is detuned and scanned to resonantly photoassociate the *B* to the *A* atoms, to form molecules. During the scan, the *B*-pulse laser power is held fixed using a proportional-integral-derivative controller (PID) [19] feedback loop that controls the rf power supplied to the 510-nm AOM. The 852-nm laser has a power of $\sim 220 \mu\text{W}$ and Gaussian waist of $\omega_{852} \simeq 80 \mu\text{m}$. The 510-nm beam has a waist $\omega_{510} \simeq 40 \mu\text{m}$ at the MOT center. The excitation region is surrounded by three pairs of field-compensation electrodes, which allow us to reduce stray electric fields to less than 250 mV/cm , via Stark spectroscopy. Rydberg atoms and molecules are detected using the electric-field ionization method (ionization ramp rise time $3 \mu\text{s}$). Alternatively, ions spontaneously generated from Rydberg atoms or molecules can be extracted with a smaller electric field. The extracted ions are detected with a microchannel plate (MCP) detector. Spontaneously formed ions and field-ionized Rydberg atoms and molecules are discriminated by their time of flight. An ion lens, consisting of three potential grids along the ion path to the MCP, is used to collimate the ions onto the MCP and to thereby optimize the ion collection efficiency.

To model Rydberg-atom macrodimers, we consider the multipole interaction, V_{int} , in the product space of two Rydberg atoms labeled *A* and *B* [16,20,21],

$$\hat{V}_{\text{int}} = \sum_{q=2}^{q_{\text{max}}} \frac{1}{R^{q+1}} \sum_{\substack{L_A=1 \\ L_B=q-L_A}}^{q_{\text{max}}-1} \sum_{\Omega=-L_A}^{L_A} f_{AB\Omega} \hat{Q}_A \hat{Q}_B$$

$$f_{AB\Omega} = \frac{(-1)^{L_B} (L_A + L_B)!}{\sqrt{(L_A + \Omega)! (L_A - \Omega)! (L_B + \Omega)! (L_B - \Omega)!}}, \quad (1)$$

where L_A and L_B are the multipole orders of atoms *A* and *B*, and $L_A <$ is the lesser of L_A and L_B ; both $L_A, L_B \geq 1$ because the atoms are neutral. For atom *A*, $\hat{Q}_A = \sqrt{4\pi/(2L_A + 1)} \hat{r}_A^{L_A} Y_{L_A}^{\Omega}(\hat{\mathbf{r}}_A)$, with radial matrix elements and spherical harmonics that depend on the Rydberg-electron position operator $\hat{\mathbf{r}}_A$. For atom *B* an equivalent expression applies, with Ω replaced by $-\Omega$. The outer sum ends at a maximum order q_{max} . We have tested cases up to $q_{\text{max}} = 6$ and found that $q_{\text{max}} = 4$ is sufficient to model potentials and level crossings with $\lesssim 1 \text{ MHz}$ accuracy. For $q_{\text{max}} = 4$, the terms included are *dd*, *do*, *od*, *dh*, *qq*, and *hd* interactions, where the first (second) letter stands for atom *A*(*B*), and *d* stands for dipole, *q* for quadrupole, *o* for octupole, and *h*

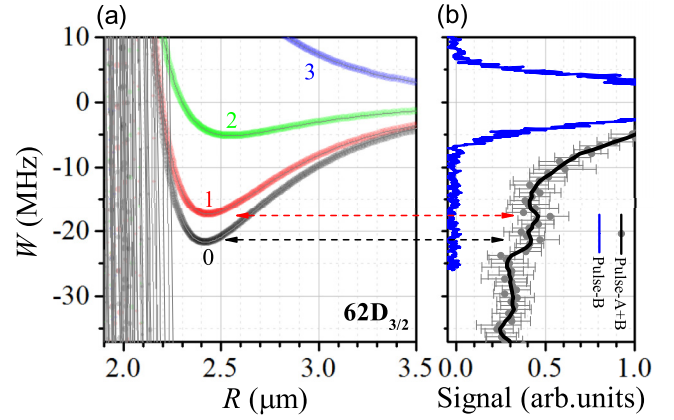


FIG. 2. (a) Calculations of adiabatic potentials (gray lines) for cesium Rydberg macrodimers $[62D_{3/2}]_2$, for the indicated values of M . Symbol areas are proportional to laser excitation rates for the experimental conditions, averaged over the random molecular alignment relative to the laboratory frame [17,22]; symbol colors correspond to different $|M|$ values. (b) Spectra measured with single-color excitation (pulse *B* only; blue line) and $[62D_{3/2}]_2$ macrodimer spectra for two-color excitation (pulses *A* and *B*; gray symbols and error bars show original data; black line shows smoothed average). Single- and two-color spectra are displayed on the same scale, with matching zero points. This also applies to Figs. 3–5 below. The peak of the single-color spectrum marks the $[62D_{3/2}]_2$ asymptote (detuning $W = 0$). Horizontal dashed lines indicate the minima of two $[62D_{3/2}]_2$ molecular potentials.

for hexadecupole interaction. Single-atom basis states were limited to quantum numbers $56.9 < n_{\text{eff}} < 62.1$, $\ell \leq 4$, and $J, |m_j| \leq 4.5$; two-body states were taken up to a maximal energy defect of 25 GHz from the $[62D_{3/2}]_2$ pair state. Due to azimuthal symmetry, the sum of the m_j values relative to the internuclear axis, $M = m_{jA} + m_{jB}$, is conserved. For $M = 0$, the number of two-body basis states is 2696. The adiabatic potentials are obtained by diagonalizing the Hamiltonian on a grid of internuclear separations, R .

Figures 2(a) and 3(a) show calculated adiabatic potentials below the $[62D_J]_2$ asymptotes for $J = 3/2$ and $5/2$, respectively, for $q_{\text{max}} = 6$, and for the relevant values of M , $|M| = 0, 1, \dots, 2J$. While most adiabatic potentials do not exhibit minima that could support bound Rydberg dimers (gray lines), all values of M , except $|M| = 2J$, support one binding potential. The binding potentials carry large oscillator strengths and exhibit minima that are up to ~ 22 and $\sim 42 \text{ MHz}$ deep, for $J = 3/2$ and $5/2$, at distances of $\sim 2.4 \mu\text{m}$. Figure 3 also shows several potentials without notable oscillator strength that intersect with the binding potentials. Close inspection of Fig. 3(a) shows that most intersections are unresolved (nonadiabatic coupling $\ll 1 \text{ MHz}$), except for $\approx 2\text{-MHz}$ -wide anticrossings at -27 MHz in both the $M = 0$ and $M = 1$ binding potentials, an $\approx 1\text{-MHz}$ -wide one at -39 MHz in $M = 1$, and a submegahertz-wide one at -35.5 MHz in $M = 2$.

To test the convergence of the calculations, we have performed more calculations with larger basis sizes. We have increased the n_{eff} range (up to $54.9 \leq n_{\text{eff}} \leq 64.9$), the $|m_j|$ range (up to $|m_j| \leq 7.5$), or the two-body energy-defect cutoff (up to 30 GHz). The basis sizes increased up to 9714 for $M = 2$

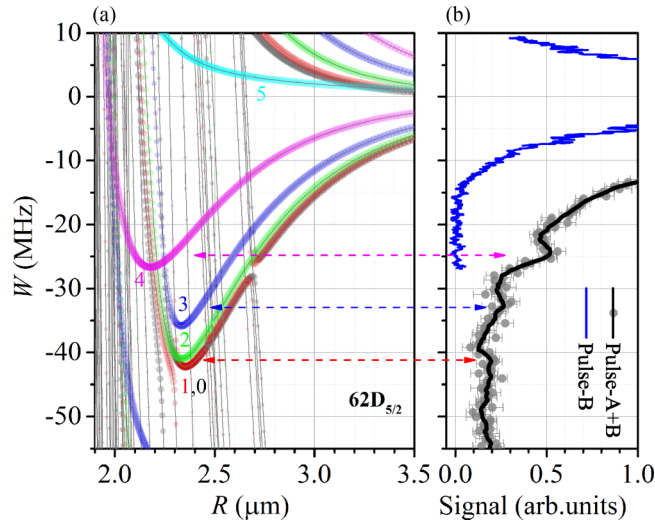


FIG. 3. (a) Calculations of adiabatic potentials for $[62D_{5/2}]_2$ macrodimers, and (b) measured spectra. The figure is analogous to Fig. 2.

(corresponding to 2×4857 symmetrized two-body states). It was found that the potential minima and energies of large oscillator strengths shift by amounts up to 10 MHz, and that the increase in $|m_J|$ range had the largest effect. To achieve convergence at the high n values used here, a supercomputer may be required. This is beyond the scope of the present work.

The black lines in Figs. 2(b) and 3(b) show two-color photoassociation spectra recorded below the $[62D_J]_2$ asymptotes. The 852-nm beam power is $210 \mu\text{W}$, and the 510-nm powers are 5.7 mW for $J = 3/2$ and 1.2 mW for $J = 5/2$. The duration of the A pulses is $0.5 \mu\text{s}$ for $J = 3/2$ and $0.2 \mu\text{s}$ for $J = 5/2$, and that of the B pulses $6.0 \mu\text{s}$ (for both J). The 510-nm powers and A-pulse durations are chosen differently to (partially) compensate the different optical excitation matrix elements for the $62D_J$ Rydberg levels. Rydberg atoms and molecules are field ionized and detected immediately after the B pulses. At detunings $|W| \gtrsim 10$ MHz the B pulses only generate a signal when the much shorter A pulses are on, i.e., if the sample is seeded with A-Rydberg-atoms. Noting that single- and two-color spectra are shown on identical scales, this observation demonstrates that the doubly-resonant photoassociation procedure is very efficient in generating Rydberg-atom pairs at large detunings.

The measured photoassociation signals in Figs. 2(b) and 3(b) include a structureless part that rapidly drops off as a function of detuning; this part is attributed to van der Waals-type interaction at distances and conditions away from the aforementioned adiabatic-potential minima. In both J cases, the measured spectra exhibit additional peaks near the minima of several of the highlighted adiabatic potentials. Most notable are the signals attributed to the $M = 3, 4$ potentials of $J = 5/2$ and the $M = 0, 1$ potentials of $J = 3/2$. These potentials also have the largest numbers of bound vibrational states, as shown next. We believe that the other potentials produce no or less significant signals because they support a lesser number of bound vibrational states ($M = 0, 1, 2$ for $J = 5/2$), or because their binding energy is so small that the signals are obscured by the atomic background signal ($M = 2$ for $J = 3/2$).

TABLE I. The rows show the measured and calculated minima of the binding adiabatic potentials of Cs $[62D_J]_2$, V_{\min} (taken by visual inspection of Figs. 2 and 3), the energy at which the number of vibrational levels is evaluated, V_{top} , the number of energy levels, N , and the average density of states (DOS) between V_{\min} and V_{top} . Energies are in MHz, and DOS in MHz^{-1} .

$M =$	0	1	2	3	4
$[62D_{3/2}]_2$					
V_{\min} , Expt.	-22 ± 2	-17 ± 2			
V_{\min} , Theor.	-21.7	-17.4	-5.1		
V_{top}	$V_{\min}/2$	$V_{\min}/2$	$V_{\min}/2$		
N	61	55	31		
DOS	5.6	6.3	12.2		
$[62D_{5/2}]_2$					
V_{\min} , Expt.	-42 ± 3	-42 ± 3	-42 ± 3	-32 ± 2	-25 ± 2
V_{\min} , Theor.	-42.2	-42.3	-41.0	-35.8	-26.7
V_{top}	-28.1	-39.6	-35.6	$V_{\min}/2$	$V_{\min}/2$
N	44	7	15	58	61
DOS	3.1	2.6	2.8	3.2	4.6

To gauge the importance of a binding potential, $V(R)$, in producing a signal indicative of metastable Rydberg dimers, the number of vibrational states below an energy V_{top} can be estimated semiclassically as $N(V_{\text{top}}) = 2 \int_{R_i}^{R_o} p(R) dR / h + 1/2$, with momentum $p = \sqrt{2\mu[V_{\text{top}} - V(R)]}$, inner and outer classical turning points $R_i(V_{\text{top}})$ and $R_o(V_{\text{top}})$, and effective mass $\mu = M_{\text{Cs}}/2 \approx 66.5u$. For the results given in Table I, we set V_{top} equal to the energies of the aforementioned anticrossings in the adiabatic potentials. Vibrational states above these anticrossings are likely unstable; we assume that they decay into fast fragments that avoid detection after the fairly long B pulse. In the cases where there are no relevant anticrossings we set $V_{\text{top}} = V_{\min}/2$ [23]. The binding adiabatic potentials with the largest numbers of metastable vibrational states and the average density of states (DOS) are expected to produce the strongest spectroscopic signals. The results in Figs. 2 and 3 and Table I support this interpretation.

Our model also yields the two-body excitation rate of two-color photoassociation of the binary molecules (methods similar to [16,20,21]). Since our sample is not optically pumped nor are the atoms spatially prearranged, the calculated rates are averaged over a random spatial distribution of positions and angles between internuclear axis and laboratory frame (defined by laser polarizations), and summed over all $|M|$. Since M values of same magnitude and opposite sign have the same spectra, the nonzero $|M|$ values are weighted twice as much as $M = 0$. Figure 4 shows comparisons between measured and calculated two-color excitation spectra on the red-detuned sides of $[62D_J]_2$. The structures in the calculated and measured spectra, indicative of the production of macrodimer Rydberg molecules, are in qualitative agreement for both cases of J .

Rydberg macrodimers are likely to undergo one or more decay processes that result in a free ion [17,24,25]. The dominant decay mode depends on the adiabatic potential the molecule is prepared on. Attractive adiabatic potentials, that are free of wells, lead to acceleration and (delayed) Penning ionization. As a second mechanism, electronic energy exchange between

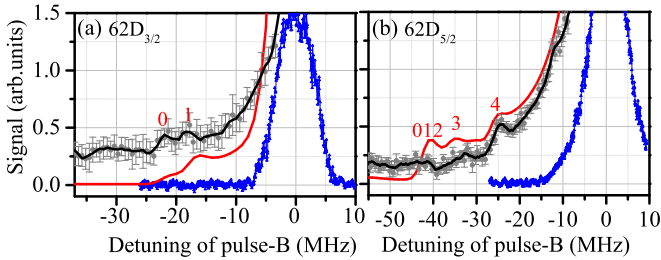


FIG. 4. Measurements and calculations (red lines) of doubly resonant two-color photoassociation spectra for $[62D_J]_2$ Rydberg molecules vs pulse- B detuning. In the calculation, the atom density is 10^8 cm^{-3} and the laser-excitation FWHM is 3 MHz. The data points (gray symbols with error bars) are measurements with seed pulse A on; the black lines show smoothed averages. The narrow signals (blue lines) are atomic reference signals with the seed pulse off. Numbers indicate the M values and the energy positions of the binding adiabatic potentials.

the constituents via long-range inter-Coulombic coupling involving continuum states [26,27] may cause molecular auto-ionization, without nuclear motion. Thirdly, potentials with wells may exhibit nonadiabatic couplings with intersecting background potentials. Nonadiabatic transitions of molecular states can cause ionization, if the intersecting potentials are attractive, or dissociation (without ionization) [28], if the intersecting potentials are repulsive. Nonadiabatic decays are particularly likely in the $J = 5/2$ case (see Fig. 3), where the binding potentials are intersected by numerous other potentials. Finally, atomic blackbody thermal ionization may add an ion background.

To detect the spontaneous ion signal that results from these ionizing interactions, after photoassociation we insert a wait time, $\tau = 10 \mu\text{s}$, during which Rydberg atoms or molecules may ionize. We then apply an electric field that is less than the ionization field for the selected atomic state; the electric field is, however, sufficient to collect any spontaneously formed ions onto the MCP. This method yields a spontaneous-molecular-ionization signal with a greatly reduced single-atom background. The blue curve in Fig. 5 shows the molecular spectrum below the $[62D_{3/2}]_2$ asymptote obtained with the ion extraction method (free-ion spectrum). For comparison, we also display the molecular signal obtained with the field-ionization method (black curve) and the one-color Rydberg excitation signal (red line). The free-ion signal drops on the blue side of the atomic resonance. This is expected due to the suppression of ionization caused by repulsive van der Waals forces on the blue side of the resonance [see repulsive potentials close to the top of Fig. 3(a)]. At large negative detunings, the free-ion signal is about half the field-ionization molecular signal. Thus, a large fraction of the Rydberg molecules excited by the A - and B -pulse sequence ionize with high probability during the waiting time (which is much shorter than the atomic lifetime). Comparison of the atomic signal with the other two curves in Fig. 5 reaffirms the high efficiency of the doubly resonant photoassociation. In view of the absence of intersecting potentials in Fig. 2(a) we believe the rapid decay of the molecular signal is due to inter-Coulombic effects (see above). Some of the ionization signal may be due to nonadiabatic couplings to potentials associated

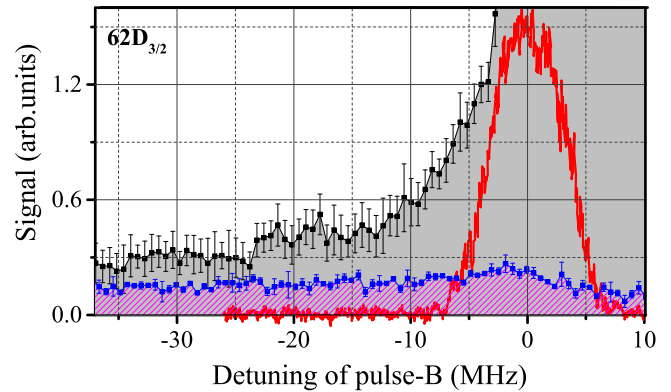


FIG. 5. Spectra of $[62D_{3/2}]_2$ macrodimers obtained with field ionization ($0 \mu\text{s}$ delay; black line) and ion extraction ($10 \mu\text{s}$ delay; blue line). For comparison, the atomic Rydberg signal is also plotted (pulse B only; red line).

with pair states outside the utilized basis sets. In Fig. 5, several peaks in the field-ionization signal may correspond to dips in the spontaneous ion signal; this indicates that the dips might correspond to longer-lived molecular resonances.

To investigate the lifetime of Rydberg-atom macrodimers, we keep the pulse- B detuning fixed at several predominant peaks in the field-ionization signals, and vary the wait time τ [see Fig. 1(c)]. For $[62D_{3/2}]_2$, at detunings near the minima in the $M = 0$ and $M = 1$ potentials, the fractions of non-ionized molecules drop on time scales of $3.0 \pm 0.3 \mu\text{s}$ and $4.0 \pm 0.4 \mu\text{s}$. For $[62D_{5/2}]_2$, at detunings near the minima in the $M = 3$ and $M = 4$ adiabatic potentials, the $1/e$ decay times are $5.5 \pm 0.7 \mu\text{s}$ and $6.8 \pm 0.9 \mu\text{s}$. These measurements provide an initial indication for the lifetimes of $[62D_J]_2$ molecules.

In conclusion, we have studied Rydberg-atom macrodimers using two-color photoassociation. The frequency difference between the two colors yields the molecular binding energy. The measured spectra agree reasonably well with calculated molecular potentials and spectra. In the future, one may study mixed-parity photoassociation schemes [17], realized by simultaneous two- and three-photon Rydberg-atom excitation. A detailed understanding of the decay modes and lifetimes of the D -state Rydberg-atom molecules will require further study; this includes the role of unresolved submegahertz nonadiabatic couplings with unbound potentials that may limit the stability of the molecular states. Also, it has been suggested that Rydberg-atom macrodimers can be used to study vacuum fluctuations [29,30], to quench ultracold collisions [14], and to measure correlations in quantum gases [15,31].

The work was supported by the National Key R & D Program of China (Grant No. 2017YFA0304203), the National Natural Science Foundation of China (Grants No. 61475090, No. 61675123, and No. 61775124), Changjiang Scholars and Innovative Research Team in University of Ministry of Education of China (Grant No. IRT13076), and the State Key Program of National Natural Science of China (Grant No. 11434007). G.R. acknowledges support by the National Science Foundation (PHY-1506093) and BAIREN plan of Shanxi province.

- [1] C. H. Greene, A. S. Dickinson, and H. R. Sadeghpour, *Phys. Rev. Lett.* **85**, 2458 (2000).
- [2] E. L. Hamilton, C. H. Greene, and H. R. Sadeghpour, *J. Phys. B* **35**, L199 (2002).
- [3] A. A. Khuskivadze, M. I. Chibisov, and I. I. Fabrikant, *Phys. Rev. A* **66**, 042709 (2002).
- [4] V. Bendkowsky, B. Butscher, J. Nipper, J. P. Shaffer, R. Löw, and T. Pfau, *Nature (London)* **458**, 1005 (2009).
- [5] V. Bendkowsky, B. Butscher, J. Nipper, J. B. Balewski, J. P. Shaffer, R. Löw, T. Pfau, W. Li, J. Stanojevic, T. Pohl, and J. M. Rost, *Phys. Rev. Lett.* **105**, 163201 (2010).
- [6] M. A. Bellos, R. Carollo, J. Banerjee, E. E. Eyler, P. L. Gould, and W. C. Stwalley, *Phys. Rev. Lett.* **111**, 053001 (2013).
- [7] D. A. Anderson, S. A. Miller, and G. Raithel, *Phys. Rev. Lett.* **112**, 163201 (2014).
- [8] A. T. Krupp, A. Gaj, J. B. Balewski, P. Ilzhöfer, S. Hofferberth, R. Löw, T. Pfau, M. Kurz, and P. Schmelcher, *Phys. Rev. Lett.* **112**, 143008 (2014).
- [9] J. Tallant, S. T. Rittenhouse, D. Booth, H. R. Sadeghpour, and J. P. Shaffer, *Phys. Rev. Lett.* **109**, 173202 (2012).
- [10] T. Niederprüm, O. Thomas, T. Eichert, and H. Ott, *Phys. Rev. Lett.* **117**, 123002 (2016).
- [11] K. S. Kleinbach, F. Meinert, F. Engel, W. J. Kwon, R. Löw, T. Pfau, and G. Raithel, *Phys. Rev. Lett.* **118**, 223001 (2017).
- [12] D. Booth, S. T. Rittenhouse, J. Yang, H. R. Sadeghpour, and J. P. Shaffer, *Science* **348**, 99 (2015).
- [13] T. Niederprüm, O. Thomas, T. Eichert, C. Lippe, J. Pérez-Ríos, C. H. Greene, and H. Ott, *Nat. Commun.* **7**, 12820 (2016).
- [14] C. Boisseau, I. Simbotin, and R. Côté, *Phys. Rev. Lett.* **88**, 133004 (2002).
- [15] K. R. Overstreet, A. Schwettmann, J. Tallant, D. Booth, and J. P. Shaffer, *Nat. Phys.* **5**, 581 (2009).
- [16] J. Deiglmayr, H. Saßmannshausen, P. Pillet, and F. Merkt, *Phys. Rev. Lett.* **113**, 193001 (2014).
- [17] H. Saßmannshausen and J. Deiglmayr, *Phys. Rev. Lett.* **117**, 083401 (2016).
- [18] C. P. Pearman, C. S. Adams, S. G. Cox, P. F. Griffin, D. A. Smith, and I. G. Hughes, *J. Phys. B* **35**, 5141 (2002).
- [19] Y. C. Jiao, J. K. Li, L. M. Wang, H. Zhang, L. J. Zhang, J. M. Zhao, and S. T. Jia, *Chin. Phys. B* **25**, 053201 (2016).
- [20] A. Schwettmann, J. Crawford, K. R. Overstreet, and J. P. Shaffer, *Phys. Rev. A* **74**, 020701 (2006).
- [21] J. Deiglmayr, *Phys. Scr.* **91**, 104007 (2016).
- [22] The apparent width of the colored lines on top of the potential curves is proportional to the square root of the oscillator strength.
- [23] Molecules higher up in energy are likely unstable due to nonadiabatic transition near the inner classical turning points and/or would be hard to discern from the atomic line.
- [24] M. Viteau, A. Chotia, D. Comparat, D. A. Tate, T. F. Gallagher, and P. Pillet, *Phys. Rev. A* **78**, 040704 (2008).
- [25] H. Saßmannshausen, F. Merkt, and J. Deiglmayr, *Phys. Rev. A* **92**, 032505 (2015).
- [26] L. S. Cederbaum, J. Zobeley, and F. Tarantelli, *Phys. Rev. Lett.* **79**, 4778 (1997).
- [27] T. Amthor, J. Denskat, C. Giese, N. N. Bezuglov, A. Ekers, L. S. Cederbaum, and M. Weidemüller, *Eur. Phys. J. D* **53**, 329 (2009).
- [28] N. Thaicharoen, A. Schwarzkopf, and G. Raithel, *Phys. Rev. A* **92**, 040701 (2015).
- [29] L. H. Ford and T. A. Roman, *Ann. Phys. (NY)* **326**, 2294 (2011).
- [30] G. Menezes and N. F. Svaiter, *Phys. Rev. A* **92**, 062131 (2015).
- [31] M. Stecker, H. Schefzyk, J. Fortágh, and A. Günther, *New J. Phys.* **19**, 043020 (2017).